Feshbach Resonances in Ultracold Atoms

A thesis is submitted in partial fulfillment of the requirement
for the degree of Bachelor of Science in Physics from
The College of William and Mary

by

Gunhee Lee

Accepted for Honors
(Honors or no-Honors)

Henry Krakauer, Director

Seth Aubin

Carey Bagdassarian

Williamsburg, VA
29, April, 2013

Feshbach Resonances in Ultracold Atoms

Isabelle Gunhee Lee

Adviser: Prof. Seth Aubin

Abstract

This thesis presents a simple theoretical model of a Feshbach resonance between two colliding ultracold atoms and experimental progress towards the observation of such a resonance in ^{85}Rb. On the theoretical side, the inter-atomic scattering potential is approximated by a spherical square well potential. The potential supports a number of bounds states whose energy depends on the width and depth of the well. In the low energy limit, only s-wave scattering is present, and the associated scattering length for the process diverges if there is a bound state at the dissociation limit: this is the hallmark of a Feshbach resonance. The model also shows that the Feshbach resonance can be shifted to higher scattering energies by adjusting the well depth, indicating the presence of a quasi-bound state above the dissociation limit. On the the experimental side, a crossed dipole trap has been developed and used to trap ultracold rubidium atoms. The performance of the trap is characterized, and the thesis describes work towards upgrading it for an experiment to observe a Feshbach resonance in the $F = 2$, $m_F = -2$ hyperfine ground state of ^{85}Rb.

1. Introduction

The objective of this project is to develop a theoretical understanding of Feshbach resonances and observe them experimentally in a gas of ultracold atoms. Feshbach resonances in ultracold atomic gases are scattering resonances in which the collision cross-section for two colliding atoms diverges for specific adjustments to the interatomic potential, generally with a magnetic field. Feshbach resonances allow

enormous control over the attractive and repulsive interactions of atoms, specifically by controlling scattering cross sections. By tuning the magnetic field, the atoms can associate into strongly interacting molecular states or dissociate as free unbound atoms. Feshbach resonances are essential for reducing interactions in a BEC interferometer and increasing those of strongly interacting superfluids [1]. Moreover, Feshbach resonances may yield advancements in more practical experiments, such as suppressing the frequency shifts of atomic clocks [2].

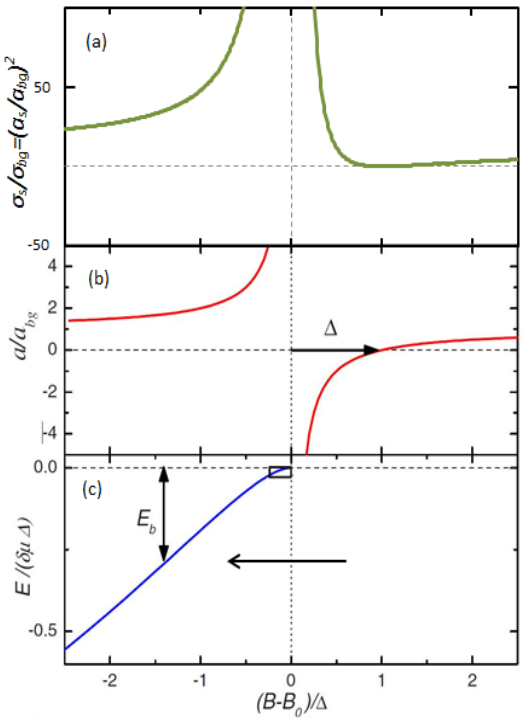

Figure 1: Cross section (a), scattering length (b), and molecular binding energy (c) of a generic Feshbach resonance. Arrow in Figure 1 (c) indicates the direction of magnetic field sweeps when creating cold molecules (adapted from reference [3]).

By definition, Feshbach resonances rely on scattering theory. A Feshbach resonance is a strong enhancement in the collision cross section and scattering length at a particular magnetic field value. As shown in Figure 1, colliding ultracold atoms experience a dramatic enhancement of their collision properties at a Feshbach resonance located at magnetic field B_0: the scattering length and cross-section diverge.

In this case, the scattering length, a_s, shown in red, is given by:

$$a_s(B) = a_{bg}(1 - \frac{\Delta}{B - B_0}) \tag{1}$$

where a_s is the s-wave scattering length, a_{bg} is the background scattering length, Δ is the width of resonance, and B_0 is the magnetic field value of resonance. At $B = B_0$ the scattering length diverges, leading to very large elastic and inelastic collision cross sections. In particular, the inelastic collisions between atoms increase at a Feshbach resonance, which leads to a trap loss, an experimental signature of a Feshbach resonance. The elastic cross section for s-wave two-body collisions is calculated using the equation (2):

$$\sigma = 4\pi {a_s}^2 \alpha \tag{2}$$

where σ is the cross section, a_s is the scattering length, $\alpha = 1$ for non-identical atoms, $\alpha = 2$ for identical bosons, and $\alpha = 0$ for identical fermions. Despite the increase in inelastic collisions at the Feshbach resonance, careful ramping of the magnetic field through the resonance (from the $a_s < 0$ side to the $a_s > 0$ side of the resonance) can produce a weak molecular bond between the colliding atoms, as shown in Figure 1 (c) [3].

Feshbach resonances provide an efficient method to producing ultracold molecules. Although Feshbach molecules themselves are extremely "fragile," Feshbach resonance association is a potentially coherent method that creates molecules in a single molecular state. Therefore, Feshbach molecules can be used as an intermediary product to producing stable molecules in a single state. Moreover, understanding Feshbach resonances may lead to advancements in studying dipolar quantum gas, ultracold chemistry, molecular interferometry, and precision measurements of fundamental symmetries [1]. The rest of the thesis is structured in the following

manner: Section 2 introduces basic concepts of scattering theory, section 3 describes the basic physics of Feshbach resonances using a toy model based on a spherical square well inter-atomic potential, and section 4 discusses the experimental work to set-up an experiment to observe a Feshbach resonance in ultracold ^{85}Rb. In conclude the thesis in section 5 by discussing prospects for future theoretical and experimental work.

2. Development of Feshbach Resonance Theory

2.1 Scattering Theory

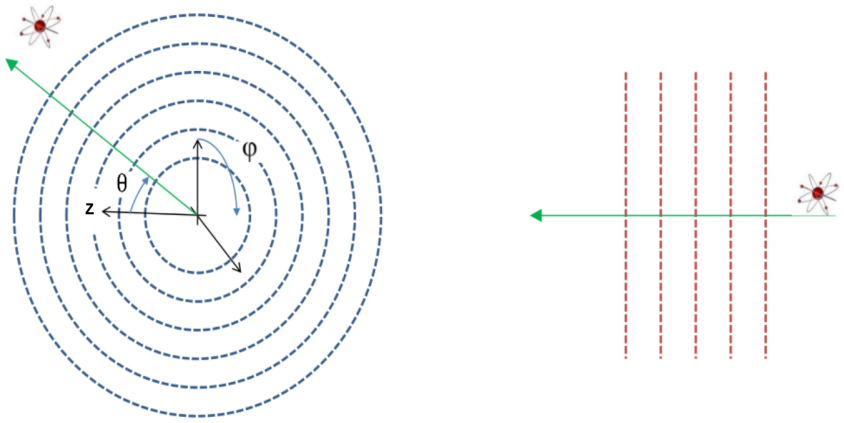

Figure 2: Basic setup of a system of two scattering atoms. The polar angle θ and azimuthal angle ϕ are defined according to the cartesian coordinate system in the diagram.

Scattering theory is essential to understanding and modeling Feshbach resonances, since Feshbach resonances are defined in terms of collisional cross sections and scattering lengths. A basic setup of scattering systems is shown in Figure 2. The setup consists of two particles colliding. If we move to the center of mass frame, a system of two colliding atoms is equivalent to a reduced incoming wave, represented as a red plane wave in Figure 2, interacting with a scattering potential and an outgoing wave, represented as a blue spherical wave. In this setup, a couple of measurements can be taken as below:

F_i = the flux of particles in the incident waves over time

$d\Omega$ = solid angle

dn =number of scattered particles per unit time

Then, dn should obviously be proportional to F_i and $d\Omega$:

$$dn = F_i \sigma(\theta, \phi) d\Omega \tag{3}$$

where σ = coefficient of proportionality. Since the potential is assumed to be spherically symmetric, the ϕ component may be omitted. Then, $\frac{d\sigma}{d\Omega}$ is defined as the differential scattering cross section. More variables of interest can be defined as we proceed, such as the scattering amplitude and the scattering length. However, a simple relation between scattering amplitude and the scattering cross section may be stated here. Scattering amplitude, denoted $f(\theta)$, in terms of the differential cross section is:

$$\frac{d\sigma}{d\Omega} = |f(\theta)|^2 \tag{4}$$

With these definitions at our disposal, the basic structure of scattering systems can be visualized. In order to understand the overarching structure, the wave equations at asymptotic limits are investigated. Assuming that the potential has essentially no effect in the asymptotic limit, the Schrodinger equation becomes:

$$\left[-\frac{\hbar^2}{2\mu}\nabla^2\right]\psi = E\psi \quad \text{(outside the influence of potential)} \tag{5}$$

where μ is the reduced mass of the potential and incoming particles, and ψ is the wave function of inter-particle separation. Then, two forms of wave equations satisfy this Schrodinger equation: an incoming plane wave and an outgoing spherical wave. Therefore, the wave equation of the system at asymptotic limits should have the

form:

$$\psi(r) \sim e^{ikz} + f(\theta)\frac{e^{ikr}}{r} \tag{6}$$

where $f(\theta)$ is defined as the scattering amplitude. We use the partial wave analysis and the phase shift of the scattered wave to determine the scattering amplitude $f(\theta)$.

2.1.1 Partial Wave Analysis

The partial wave analysis constructs solutions of the scattering systems using defined partial waves as a basis set. The partial waves are the solutions that satisfy the radial Schrodinger equation near the potential. In this case, the partial waves are spherical hankel functions of the first kind:

$$h_l^{(1)}(x) \equiv j_l(x) + in_l(x) \tag{7}$$

Hankel functions are a valid basis set, since in the $x \to +\infty$ asymptotic limit, they behave like spherical waves:

$$\lim_{x\to\infty} h \to (-i)^{l+1}\frac{e^{ikr}}{kr} \tag{8}$$

Since the potential is spherically symmetrical, the resulting solution is:

$$\psi(r,\theta) = A\left\{e^{ikz} + k\sum_{l=0}^{\infty} i^{(l+1)}(2l+1)a_l h_l^{(1)}(kr)P_l(\cos\theta)\right\} \tag{9}$$

where A is a general constant, and a_l is the amplitude of the spherical partial wave with angular momentum l. Then, from (8) and (9), the scattering amplitude can be found:

$$f(\theta) = \sum_{l=0}^{\infty}(2l+1)a_l P_l(\cos\theta) \tag{10}$$

2.1.2 Phase Shift

As shown in the previous section, the amplitudes of the incoming waves and outgoing waves are different. However, in order to maintain conservation of particle number in each angular momentum channel l (elastic scattering), the norms of incoming and outgoing waves must be the same, so this difference in amplitudes can be represented as a difference in phase instead: the outgoing wave is out of phase with the incoming wave by a factor of $2\delta_l$. Then, the scattered wave can be written solely in terms of phase $2\delta_l$. First, the incoming plane waves are written in terms of spherical waves, using Rayleigh's formula:

$$\psi_{incident} = e^{ikz} = \sum_{l=0}^{\infty} i^l (2l+1) j_l(kr) P_l(\cos\theta) \tag{11}$$

Multiplying the outgoing spherical component of (11) by phase component ($e^{2i\delta}$), the equation becomes:

$$\psi_{incident} = \sum_{l} A \frac{2l+1}{2ikr} \left[e^{i(kr+2\delta)} - (-1)^l e^{-ikr} \right] P_l(\cos\theta) \tag{12}$$

Using (10), the outgoing scattered wave can be represented as:

$$\psi_{scattered} = \sum_{l=0}^{\infty} (2l+1) a_l P_l(\cos\theta) \frac{e^{ikr}}{r} \tag{13}$$

As mentioned before, since phase shift is another way of representing the difference in amplitudes, the scattering amplitude can be written in terms of phases by matching equation (12) and (13):

$$A \sum_{l=0}^{\infty} \frac{2l+1}{2ik} P_l(\cos\theta)(e^{2i\delta_l} - 1) = A \sum_{l=0}^{\infty} (2l+1) a_l P_l(\cos\theta) \tag{14}$$

and simplifying (14),

$$\sum_{l=0}^{\infty} a_l = \sum_{l=0}^{\infty} \frac{1}{k} e^{i\delta_l} \sin \delta_l \tag{15}$$

Plugging (15) into (10), the scattering amplitude becomes:

$$f(\theta) = \frac{1}{k} \sum_{l=0}^{\infty} (2l+1) e^{i\delta_l} \sin \delta_l P_l(\cos \theta) \tag{16}$$

2.1.3 Scattering Length

The phase shift approach is particularly convenient, because it is directly connected to the scattering length, usually denoted a_s. The scattering length is defined as the s-wave limit of the equation (15). In the s-wave limit, the angular term l is 0, and k approaches 0. The s-wave limit is highly relevant to this project, since the collision of ultracold atoms only involves $l = 0$ terms. Then, equation (15) becomes:

$$a_s = -\lim_{k \to 0} \left[\frac{1}{k} e^{i\delta_0} \sin \delta_0 \right] \tag{17}$$

Moreover, another useful variable can be defined in terms of the scattering length, which is the scattering cross section. Since $\frac{d\sigma}{d\Omega} = |f(\theta)|^2$, the total scattering cross section σ becomes:

$$\sigma = \int \frac{d\sigma}{d\Omega} d\Omega = \int |f(\theta)|^2 d\Omega = \int \frac{1}{k^2} \sin^2 \delta_0 d\Omega = \frac{4\pi}{k^2} \sin^2 \delta_0 \tag{18}$$

Taking the limit as k approaches 0,

$$\sigma = 4\pi a_s^2 \tag{19}$$

Example: Hard Sphere Scattering

An example relevant to Feshbach resonances is a hard sphere scattering and its scattering length. Hard sphere scattering is defined by the potential:

$$V = \begin{cases} 0, & \text{if } r > R. \\ \infty, & \text{if } r < R. \end{cases} \tag{20}$$

The radial schrodinger equation of this potential is clearly $u(r) = A\sin(kr + \delta_0)$. The boundary condition of this potential becomes $u(R) = 0$, for the radial wave equation $u(r)$. In order for the wave equation to satisfy the boundary condition, $\delta_0 = -kR$. Then, in the case of hard sphere scattering, the scattering length becomes:

$$a_s = -\lim_{k\to 0}\left[\frac{1}{k}e^{-ikR}\sin(-kR)\right] \simeq \frac{1}{k}(1+ikR)kR \simeq R \tag{21}$$

Then, the scattering cross section follows from (19):

$$\sigma = 4\pi R^2 \tag{22}$$

3. The Feshbach Resonance Toy Model

One of the major theoretical objectives is to make a toy model of Feshbach resonances that explains the basic physics. Feshbach resonances occur when the atoms encounter a bound state energy level that is almost unbounded. In order to investigate further, we need to understand bound states better. However, the molecular potential energy is complicated to model, so we replace it with a simpler potential that still retains the basic physics we are interested in: we approximate the internuclear molecular potential with a square well potential for studying collisions between two identical ground state atoms. In particular, we focus on the scattering behavior of the atoms when the well barely spports a bound state, which is the reported condition for a Feshbach resonance. In this section, we first study the bound states on the one-dimensional square well potential, which we then apply to the determination of the s-wave bound states of the three-dimensional spherical square well potential. Second, we investigate s-wave scattering from this spherical

well potential and determine the dependence of the scattering phase shift δ_0 and scattering length a_s on the well parameters. Finally, we investigate the Feshbach resonances of this spherical well potential.

3.1 1-D Square Well Potential

In order to investigate bound states, bound states of a square well are studied. The energy levels of the system are calculated, as the well depth varies from shallow to deep. Figure 3 plots the potential of the system as a function of position.

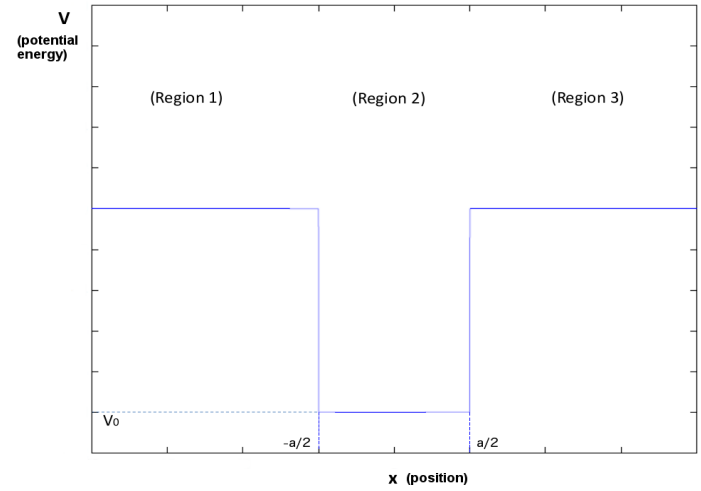

Figure 3: Potential of an Attractive Well

Dividing the system as shown in Figure 3, the Schrodinger equations of respective regions are as follows:

$$-\frac{\hbar^2}{2m}\frac{\partial^2}{\partial x^2}\psi = E\psi \qquad \text{(Region 1 and 3)} \tag{23}$$

$$\left[-\frac{\hbar^2}{2m}\frac{\partial^2}{\partial x^2} - V_0\right]\psi = E\psi \qquad \text{(Region 2)} \tag{24}$$

Moreover, we define

$$k = \sqrt{\frac{2m(E+V_0)}{\hbar^2}} \tag{25}$$

$$k_0 = \sqrt{\frac{2mV_0}{\hbar^2}} \tag{26}$$

From equations above, the boundary conditions are derived:

$$\left|\sin\left(\frac{ka}{2}\right)\right| = \frac{k}{k_0} \quad \text{for} \tan\left(\frac{ka}{2}\right) < 0 \tag{27}$$

$$\left|\cos\left(\frac{ka}{2}\right)\right| = \frac{k}{k_0} \quad \text{for} \tan\left(\frac{ka}{2}\right) > 0 \tag{28}$$

Equations (27) and (28) cannot be solved analytically, so these are solved graphically as shown in Figure 4. y_1 and y_2 in the figures are defined as:

$$y_1 = \begin{cases} \left|\sin\left(\frac{ka}{2}\right)\right|, & \text{if } \tan\left(\frac{ka}{2}\right) < 0. \\ \left|\cos\left(\frac{ka}{2}\right)\right|, & \text{if } \tan\left(\frac{ka}{2}\right) > 0. \end{cases} \tag{29}$$

$$y_2 = \frac{k}{k_0} \tag{30}$$

As V_0 increases, or as the well deepens, the number of solutions, represented by the intersection points, increases. This signifies that the number of available energy levels, or bound states of the system, increases as well.

In order to investigate the behavior of the bound state energies further, the energies are plotted as the potential is scanned from $V_0 = 1$ to $V_0 = 120$. First, the solutions are found computationally, using intersections. As shown in Figure 4 the solutions are given as k values, and they are converted to energies using the equation below:

$$E = \frac{\hbar^2}{2m}(k^2 - k_0^2) \tag{31}$$

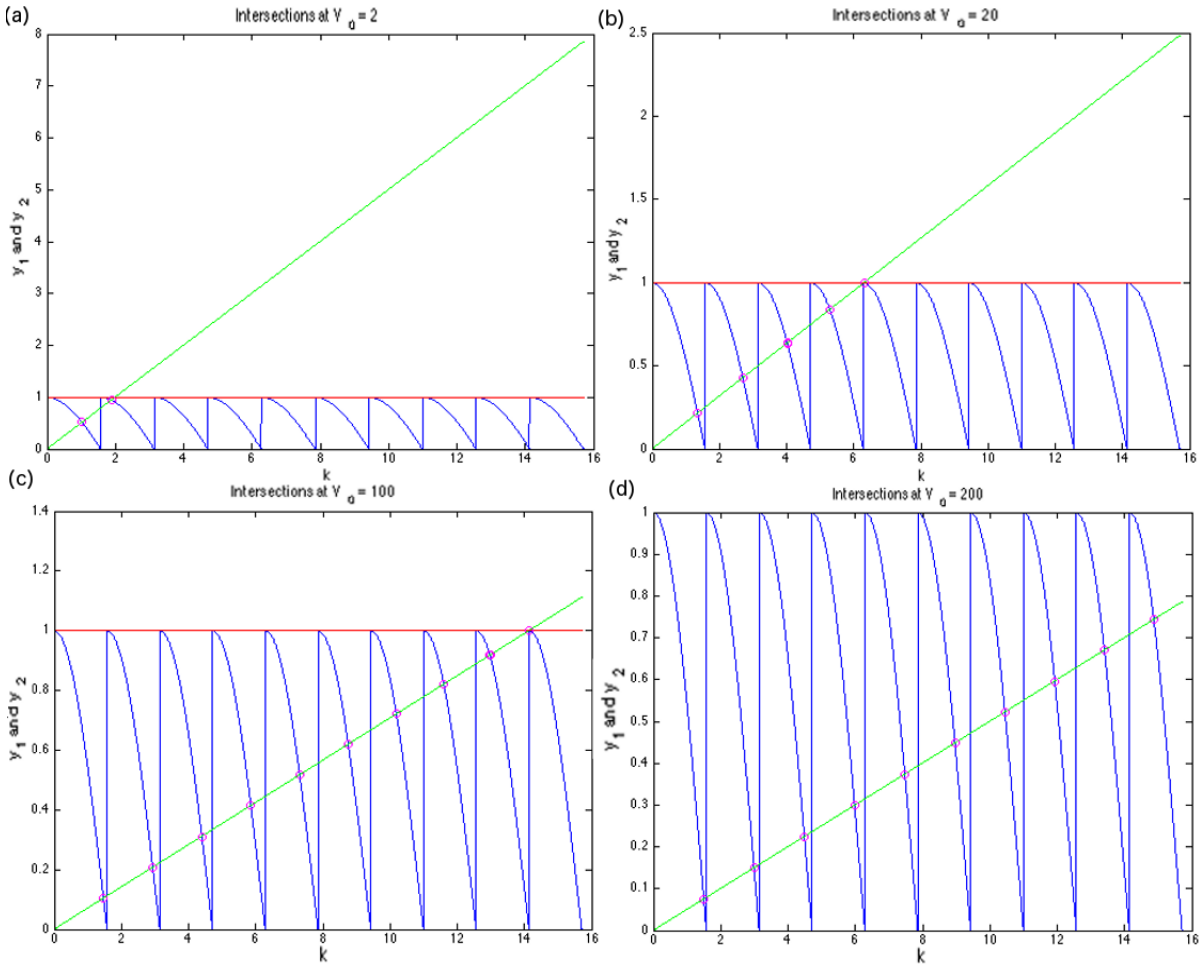

Figure 4: Plots of the boundary conditions (29) and (30) as the well depth (V_0) increases. The intersections are the bound state solutions in terms of k. The plots are for (a) $V_0 = 2$, (b) $V_0 = 20$, (c) $V_0 = 100$, and (d) $V_0 = 200$. For this plot, $\hbar$ is set to 1, m is set to 1, and a is set to 2. y_1 is in blue, and y_2 is in green. The circles are the intersections of the two boundary conditions. So, they represent at which k the boundary conditions are satisfied.

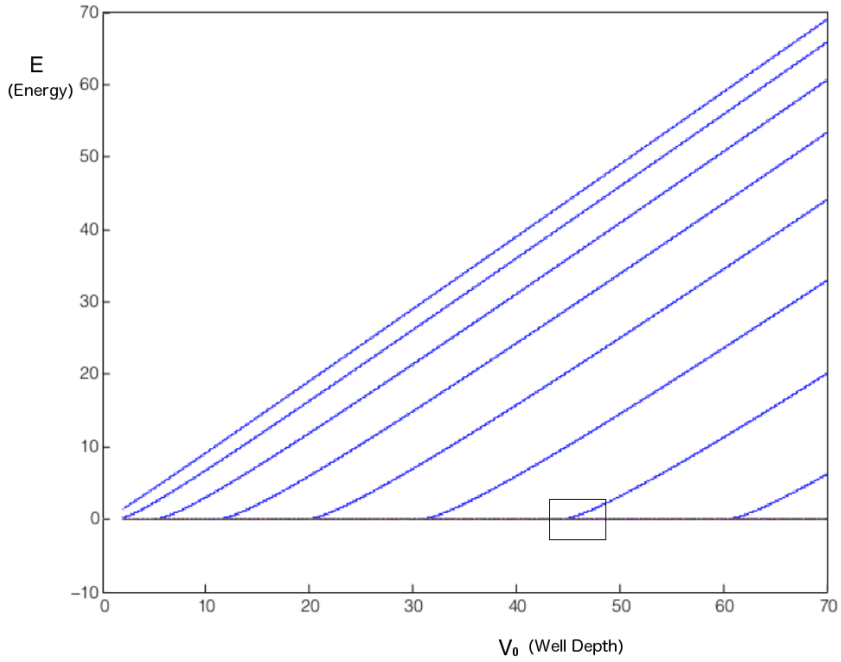

Figure 5: Bound state energies versus the depth of the well. For this plot, $\hbar$ is set to 1, m is set to 1, and a is set to 2.

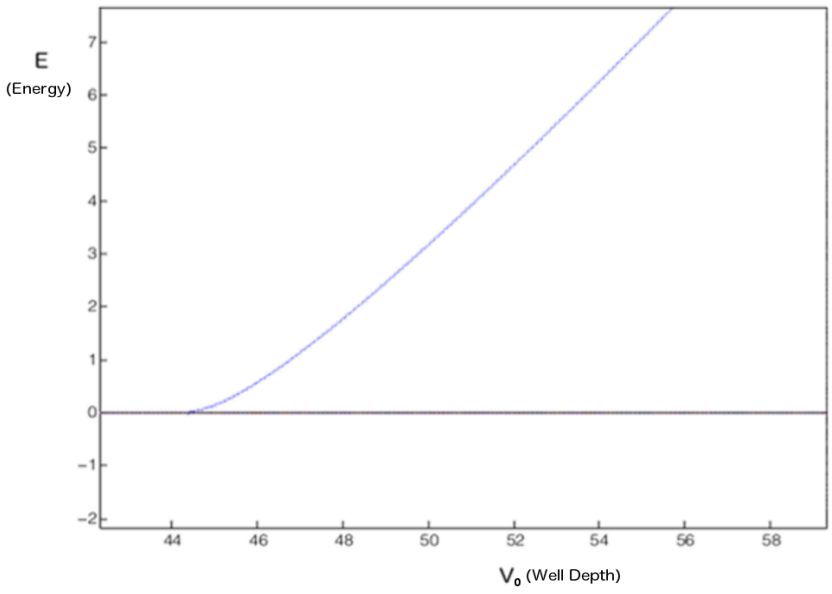

Figure 6: Close-up of the boxed portion of Figure 5

Then, these energies are plotted against the varying potential, and Figure 5 is the resulting plot. The energy levels exhibit discrete behavior: new energy levels appear at distinctive well depths, as shown in Figures 5 and 6.

The square well potential is highly relevant to our toy model for Feshbach resonances, since varying well depth is analogous to the varying potential created by sweeping magnetic fields in Feshbach resonances. Thus, understanding and modeling attractive well energy levels is a first look at modeling bound states of Feshbach resonances. The plots are generated by Matlab codes in Appendix A.1.

3.2 Spherical Well Potential

In order to study the phase shifts, a spherical well potential is studied. The spherical well potential is given by the equation below:

$$V(r) = \begin{cases} -V_0, & \text{if } r < r_0. \\ 0, & \text{if } r > r_0. \end{cases} \tag{32}$$

Then, the Schrodinger equations of the system becomes:

$$\left[-\frac{\hbar^2}{2m}\nabla^2 - V_0 \right] \psi = E\psi \quad \text{if } r < r_0 \tag{33}$$

$$-\frac{\hbar^2}{2m}\nabla^2\psi = E\psi \quad \text{if } r > r_0 \tag{34}$$

As particles encounter and interact with this potential and scatter they gain a phase. Then, the system of wave functions that satisfy the Schrodinger equations (33) and (34) will be the linear combination of the initial wave and the phase shifted scattered wave. Denoting phase as δ, the radial compotnents of the solutions become, for angular momentum $l = 0$:

$$u(r) = \begin{cases} A\sin(k'r) & \text{if } r < r_0. \\ B\sin(kr+\delta) & \text{if } r > r_0. \end{cases} \tag{35}$$

where

$$k = \frac{\sqrt{2mE}}{\hbar} \tag{36}$$

and

$$k' = \frac{\sqrt{2m(E+V_0)}}{\hbar}. \tag{37}$$

Combining equations (36) and (37),

$$\frac{k'^2}{2m} - V_0 = \frac{k^2}{2m} \tag{38}$$

3.2.1 Spherical Well Bound states

From the continuity of the wave functions and their derivatives at $r = r_0$, the boundary condition becomes:

$$\cot(k'r_0) = -\frac{k}{k'} \tag{39}$$

Then, we may define two functions, y_1 and y_2:

$$y_1 = \cot(k'r_0) \tag{40}$$

$$y_2 = -\frac{k}{k'} \tag{41}$$

Using the same methods as with square well potential, the intersections of y_1 and y_2 are found, as V_0 is scanned. The resulting plots are shown in Figure 7:

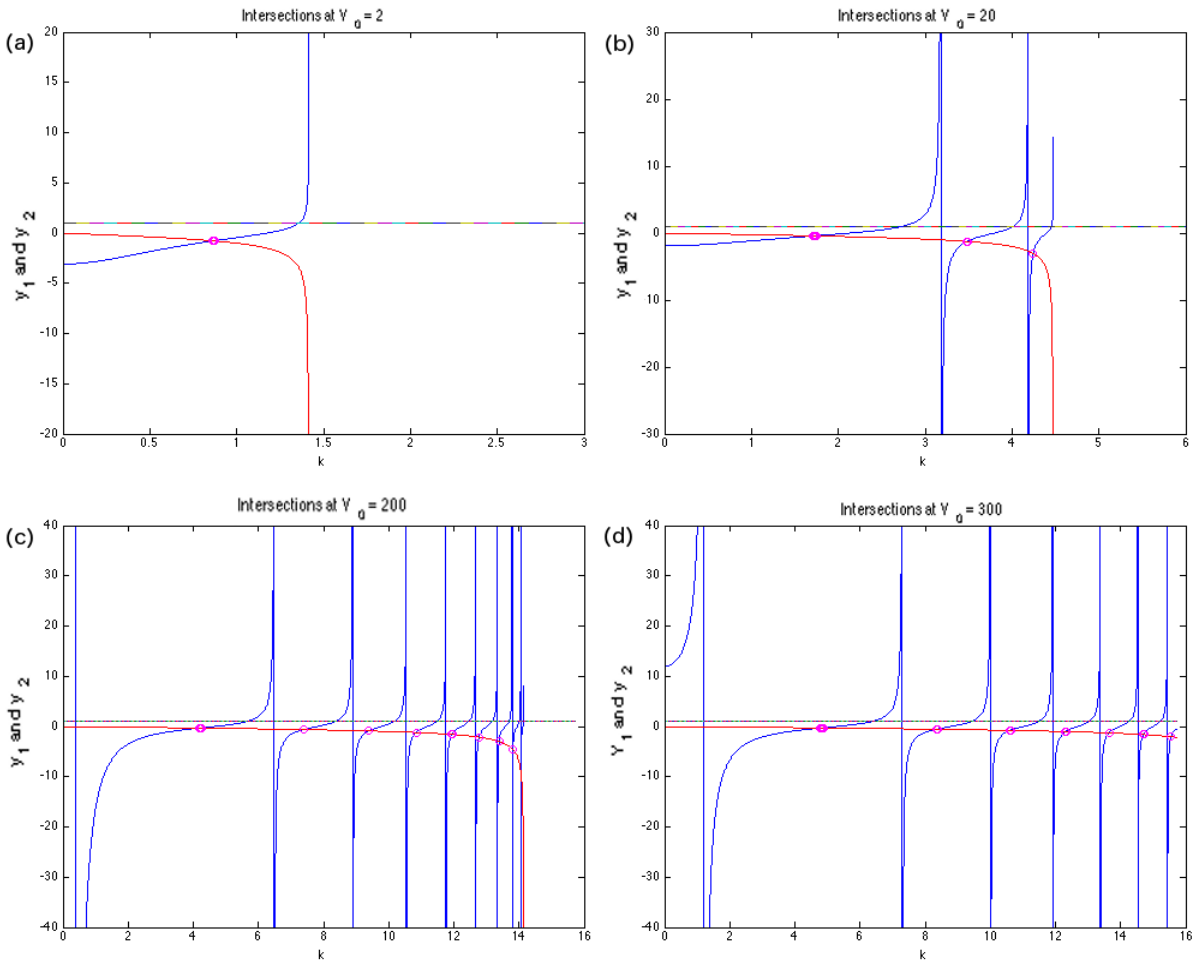

Figure 7: Intersections of y_1 and y_2 at varying values of V_0. y_1 is in blue, and y_2 is in red. $V_0 = 2$ for (a), $V_0 = 20$ for (b), $V_0 = 200$ for (c), and $V_0 = 300$ for (d). The circles represent the intersections of y_1 and y_2. So, they represent at what k the boundary conditions are satisfied. For this plot, $\hbar$, m, and r_0 are set to 1.

Then, converting the resulting k values of the intersections to energy, the E vs. V_0 plot is created as below.

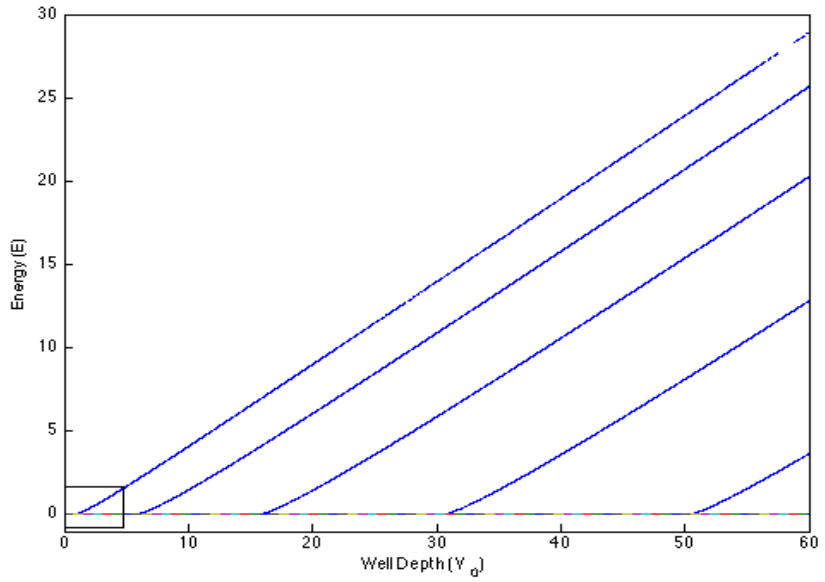

Figure 8: E vs. V_0. Bound state Energies as a function of the Well Depth. For this plot, $\hbar$, m, and r_0 are set to 1.

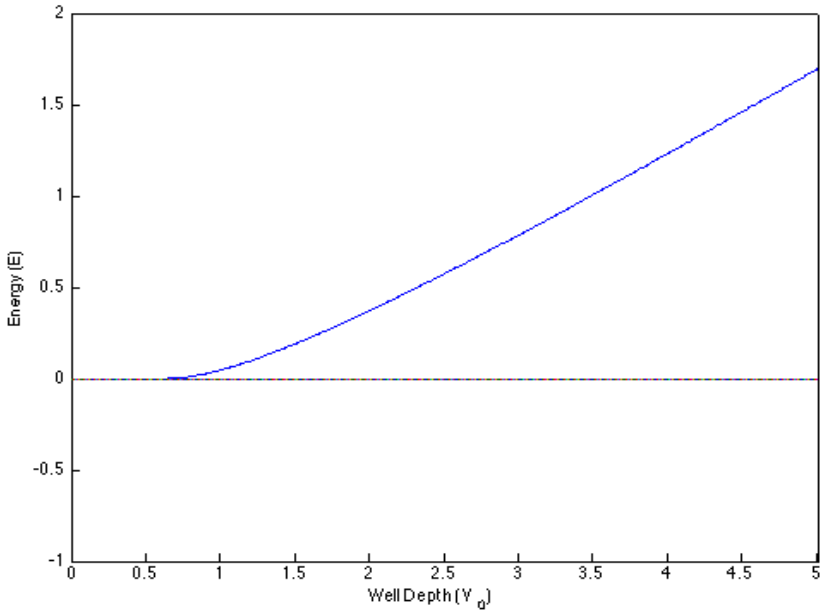

Figure 9: Close-up of the boxed portion of Figure 8. For this plot, $\hbar$, m, and r_0 are set to 1.

Similar to the square well potential, the bound state energies occur at discrete

values of the well depth V_0, as shown in Figure 8. The plots are generated by Matlab codes in Appendix A.2.

3.2.2 Spherical Well Potential Scattering

In order to determine the scattering amplitude for $k \to 0$ and $l = 0$, another boundary condition for the system can be derived, using phase shifts. From equation (38) and the continuity of the wave functions and their derivatives at $r = r_0$ requires that

$$k' \cot(k' r_0) = k \cot(k r_0 + \delta) \tag{42}$$

Solving above for δ yields an implicit expression:

$$\tan \delta = \frac{k \sin k' r_0 \cos k r_0 - k' \sin k r_0 \cos k' r_0}{k' \cos k' r_0 \cos k r_0 + k \sin k r_0 \sin k' r_0} \tag{43}$$

Since the above equation cannot be solved explicitly, it is solved using numerical methods. The phase δ is plotted against k, as shown in Figure 10.

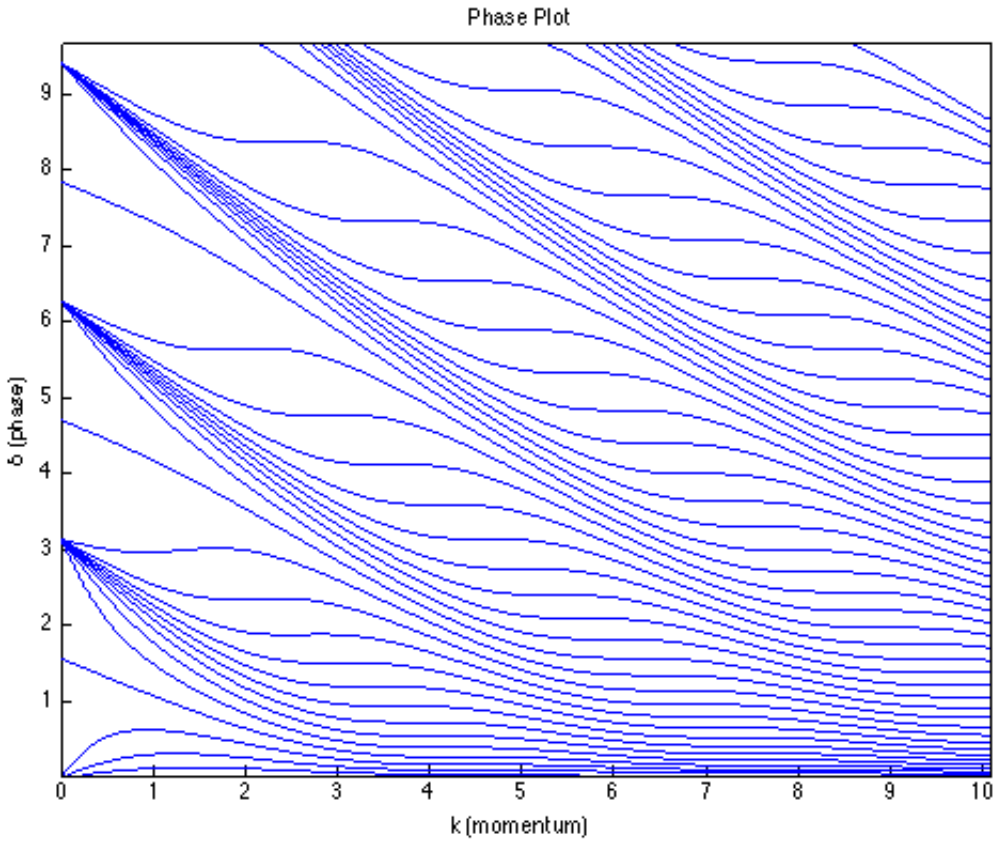

Figure 10: Phase δ vs. k at varying values of V_0. Since $V_0 = q^2/2m$, V_0 is varied by scanning q. Each line represents a solution for a different value of q, starting at $q = 0$ and increasing in steps of $\Delta q = 0.1$ This result matches the phase plot of [8].

Each line of the plot represents phase as a function of k, $\delta(k)$ at varying V_0. For simplicity, we define $V_0 = q^2/2m$ where q is a parameter with units of momentum. Then, q is numerically scanned to plot each line of Figure 10. Figure 10 suggests that the phase displays a discrete behavior, similar to energy. The plot is generated by Matlab codes in Appendix A.3.

3.3 Scattering Length Plot

The definition of scattering length is given by (17). Equation (17) can be rearranged to yield an equivalent definition of the scattering length:

$$a_s = -\lim_{k \to 0} \frac{\tan \delta}{k} \tag{44}$$

The numerical solution of (43) illustrated in Figure 10 provides function of phase in terms of k, $\delta(k)$. Then, $\delta(k)$ of Figure 10 can be used to numerically solve for the scattering length. By setting $k = 0.001$ at varying values of V_0 in Figure 10, solving for $\tan \delta / k$, and plotting the resulting points, we attain the points in Figure 11. Then, the points are fitted with the function:

$$a_s = -\frac{1}{V_0 - 1.2324} \tag{45}$$

This function is very similar to equation (1) that characterizes the behavior of atoms at Feshbach resonances. Similar to (1), (45) has a basic structure of (constant)/(x - constant). This result indicates that a Feshbach resonance can be modeled using the spherical well potential, thus validating our choice of toy model.

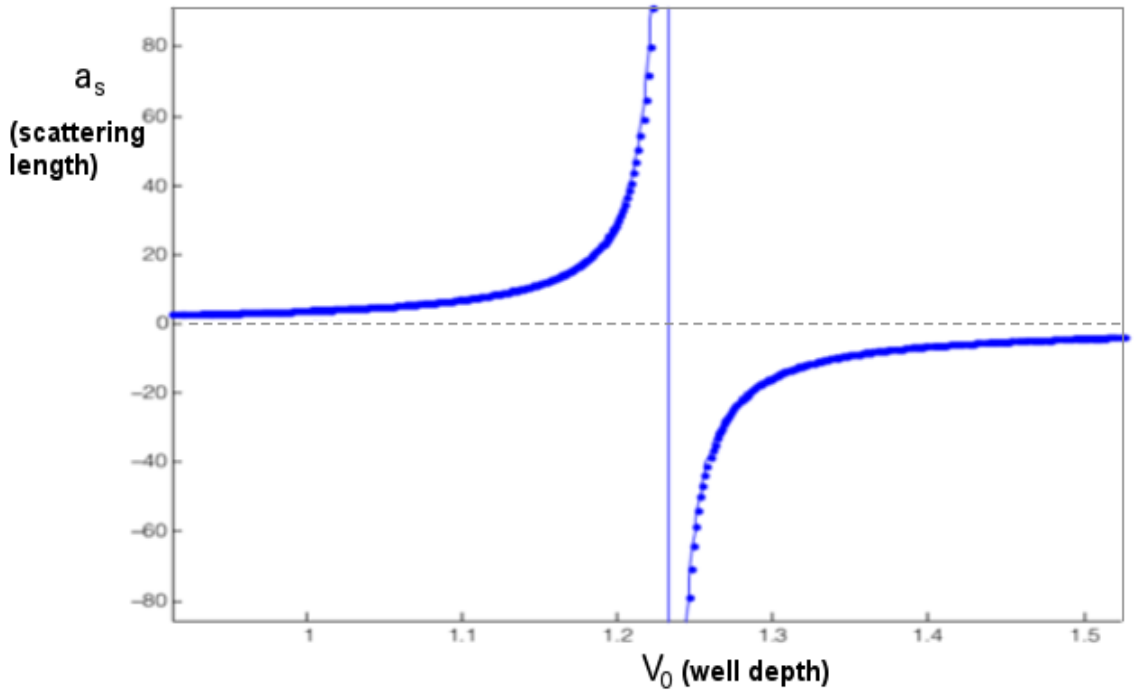

Figure 11: Scattering length vs. well depth (a_s vs. V_0). The momentum k is set to 0.001. For this plot, $\hbar$, m, and r_0 are set to 1.

This plot is generated by Matlab codes in Appendix A.4.

3.3.1 Analytical Solution of the Scattering Length

While it is numerically confirmed that Feshbach resonances can be modeled using the spherical well potential, the equation for scattering length of (1) can be also analytically derived from the implicit expression for δ in terms of k in (43). Dividing equation (43) by k, we obtain

$$\frac{\tan\delta}{k} = \frac{k\sin k'r_0\cos kr_0 - k'\sin kr_0\cos k'r_0}{k'k\cos k'r_0\cos kr_0 + k^2\sin kr_0\sin k'r_0} \tag{46}$$

Then, using (44) and (46), the scattering length becomes:

$$a_s = -\lim_{k\to 0}\frac{\tan\delta}{k} = -\lim_{k\to 0}\frac{k\sin k'r_0\cos kr_0 - k'\sin kr_0 cos k'r_0}{k'k\cos k'r_0\cos kr_0 + k^2\sin kr_0\sin k'r_0} \tag{47}$$

$$= -\frac{\sin k'r_0}{k'\cos k'r_0} + \lim_{k\to 0}\frac{\sin kr_0}{k}\cdot\frac{r_0}{r_0}\cdot\lim_{k\to 0}\frac{k'\cos k'r_0}{k'\cos k'r_0\cos kr_0 + k\sin kr_0\sin k'r_0} \tag{48}$$

$$= -\frac{\tan k'r_0}{k'} + r_0 \tag{49}$$

Using the definition of k', the limit of k' as a function of V_0 becomes as follows:

$$\lim_{k\to 0} k' = \lim_{k\to 0}\sqrt{k^2 + 2mV_0} = \sqrt{2mV_0} \tag{50}$$

Then, substituting (50) into (49),

$$a_s = -\frac{r_0\tan r_0\sqrt{2mV_0}}{r_0\sqrt{2mV_0}} + r_0 \tag{51}$$

Defining $\phi = r_0\sqrt{2mV_0}$,

$$a_s = -\frac{r_0\tan\phi}{\phi} + r_0 \tag{52}$$

Feshbach resonances are defined by dramatic increases or divergences of scattering lengths at particular magnetic field values. Since $\tan\phi$ has divergences at $(n{+}1)\pi/2$, (52) is series expanded at $\phi = \pi/2$ as below:

$$a_s = r_0\left[-\frac{2}{\pi(\phi - \pi/2)} + \frac{4}{\pi^2} + \mathcal{O}(x - \pi/2)^n\right] + r_0 \tag{53}$$

Ignoring terms other than the Laurent term of the tangent expansion, the scattering length becomes:

$$a_s = r_0\left[-\frac{2}{\pi(\phi - \pi/2)}\right] + \left(\frac{4}{\pi^2} + 1\right)r_0 \tag{54}$$

We may ignore other terms, because at divergences, the Laurent terms will dominate. Substituting $\phi = r_0\sqrt{2mV_0}$, the scattering amplitude is finally expressed in

terms of the well depth:

$$a_s = r_0 \left[-\frac{2}{\pi(r_0\sqrt{2mV_0} - \pi/2)} \right] + \left(\frac{4}{\pi^2} + 1 \right) r_0 \tag{55}$$

Equation (55) has the basic components of equation (1). Since the series expansion only holds near the divergence at $\pi/2$, (55) is a local descriptor of the scattering length, as is (1). This analytically confirms that the Feshbach resonances can be modeled from scattering of spherical well potential. This can be explained, because the applied magnetic field used to trapped atoms creates potential that resembles the spherical well potential.

Moreover, (55) can be generalized for all divergences, since tangent is divergent at $(2n+1)\pi/2$.

$$a_s = r_0 \left[-\frac{2}{(2n+1)\pi(r_0\sqrt{2mV_0} - (2n+1)\pi/2)} \right] + \left(\frac{4}{\pi^2} + 1 \right) r_0 \tag{56}$$

3.3.2 Feshbach Resonance Dependence on Well Depth

Since the divergences occur at $\phi = \frac{(2n+1)\pi}{2}$, this implies:

$$\phi = r_0\sqrt{2mV_0} = \frac{(2n+1)\pi}{2} \tag{57}$$

Thus, the divergences occur for well depths at:

$$V_0 = \frac{(2n+1)^2\pi^2}{8mr_0^2} \tag{58}$$

This equation (58) is verified numerically. From the numerical model of Figure 11, the well depths at which Feshbach resonances occur are identified and plotted against n, as shown in Figure 12. Then, (58) is used as a fitting function for the points. The resulting plot below verifies that (58) holds.

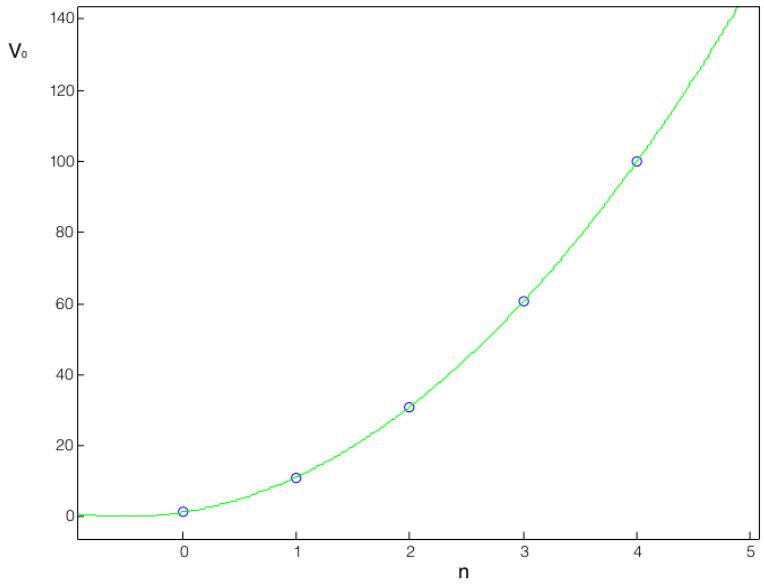

Figure 12: Well depths at which Feshbach resonances occur for discrete n. The analytical solution (58) is in green. For this plot, $\hbar$, m, and r_0 are set to 1.

3.4 Feshbach Resonance at Finite Momentum

From 2.1.2, the scattering length is defined in terms of the limit below:

$$a_s = -\lim_{k\to 0}\left[\frac{1}{k}e^{i\delta_0}\sin\delta_0\right] \tag{59}$$

In section 3.3, the numerical plot of the scattering length and the well depth, Figure 11, is obtained by scanning V_0 and plotting the equation below at $k = 0.001$:

$$a_s(k) = -\frac{1}{k}e^{i\delta_0}\sin\delta_0 \tag{60}$$

In this section, the scattering lengths at finite momenta are investigated. The cases at $k = 0.499$, $k = 0.99$ are investigated in Figure 13 (b) and (c).

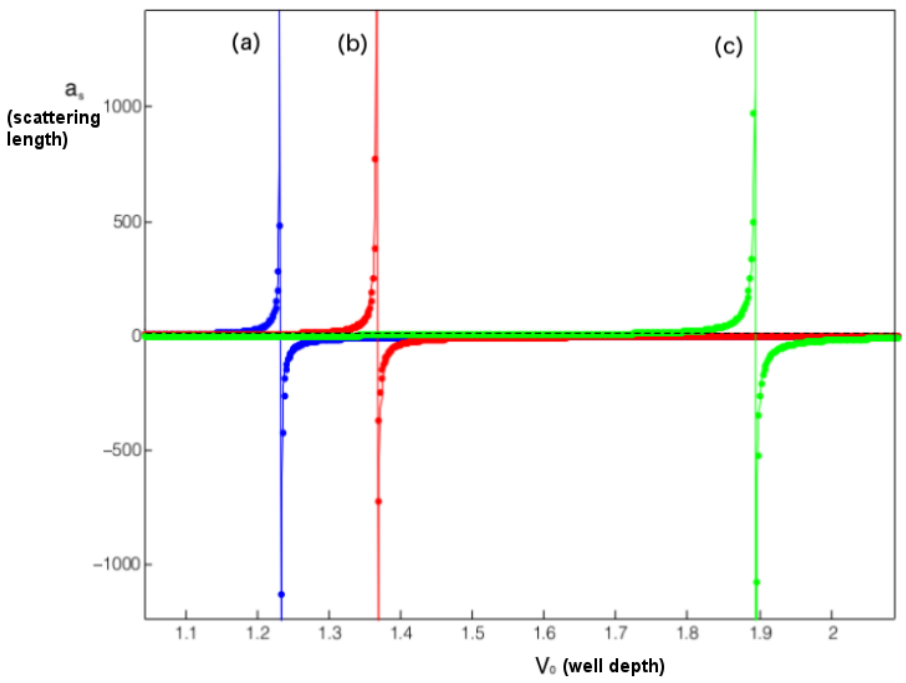

Figure 13: Shifts in scattering lengths for finite momentum. For (a), $k = 0.001$, for (b), $k = 0.4990$, and for (c), 0.999. For this plot, $\hbar$, m, and r_0 are set to 1.

The fitting function for Figure 13 (a) is:

$$a_s = -\frac{1}{V_0 - 1.2324} \tag{61}$$

The fitting function for Figure 13 (b) is:

$$a_s = -\frac{1}{V_0 - 1.3660} \tag{62}$$

The fitting function for Figure 13 (c) is:

$$a_s = -\frac{1}{V_0 - 1.8935} \tag{63}$$

Figure 13 illustrates that Feshbach resonances shift to the right as momenta increase

from near 0. The plot is generated by Matlab codes in Appendix A.4.

4. Experiment

The long term experimental objective of this project is the observation of a magnetic Feshbach resonance. The basic experimental approach is to load μK-level ultracold atoms into an optical dipole trap, and the subject them to a magnetic field. The Feshbach resonance is identified by observing the trap lifetime, or loss rate, at different magnetic field strengths. An unusually large loss rate, or short lifetime indicates a magnetic Feshbach resonance.

4.1 Candidates

Table 1. Candidates and Feshbach Resonances

Type	B (G)	Δ (G)	States	Sources
^{85}Rb (boson-boson)	155	11.65	$\|2,-2>+\|2,-2>$	[4]
^{39}K-^{87}Rb (boson-boson)	117.6	-1.3	$\|1,-1>+\|1,-1>$	[5]
^{39}K-^{87}Rb (boson-boson)	247.9	0.28	$\|1,1>+\|1,1>$	[5]
^{39}K-^{87}Rb (boson-boson)	318	7.6	$\|1,1>+\|1,1>$	[5]
^{41}K-^{87}Rb (boson-boson)	49.5	-6.5	$\|2,2>+\|2,1>$	[6]
^{41}K-^{87}Rb (boson-boson)	53.5	-39	$\|1,1>+\|1,1>$	[6]
^{41}K-^{87}Rb (boson-boson)	87.5	-1.3	$\|1,1>+\|1,1>$	[6]
^{40}K-^{87}Rb (fermion-boson)	545.4	1.2		[7]

Originally, ^{87}Rb, ^{85}Rb, and ^{39}K atoms were considered for the experiment. More specific groupings of these atoms are identified from the literature, as shown in Table 1. B is the magnetic field at which Feshbach resonance is observed for the corresponding atom pair, and Δ is the width of resonance. In order to ensure the observation of Feshbach resonances, pairs with wider width of resonances are selected. Pairs with relatively low magnetic fields, around 150G to 200G, are also preferred. Based on the available isotope and magnets, the experiment will be done using ^{85}Rb.

4.2 Basic Experimental Setup

The basic experimental setup is described in Figure 14. The MOT, or the magneto-optical trap, laser cools the atoms to 10 to 100 μK range. Then, the dipole trap is constructed, because the dipole trap is not sensitive to varying magnetic fields. The dipole trap is an intense, far off-resonance, conservative laser trap that can operate at arbitrary magnetic field. The trap potential energy is proportional to the laser intensity. The experimental setup is also shown in Figure 14. By sweeping the magnetic field near a Feshbach resonance, which is represented as B_{feshbach} in Figure 14, there would be a loss of atoms. The atom losses most likely are due to an increase in inelastic collisions between atoms at the resonances, an experimental signature of Feshbach resonances.

4.3 Initial Dipole Trapping Result

The dipole trap is first constructed using ^{87}Rb as shown in Figure 14.

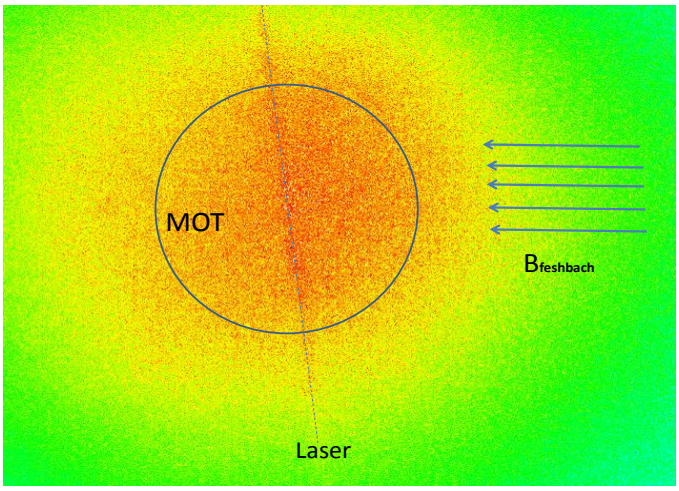

Figure 14: Constructed MOT and Dipole Trap using ^{87}Rb, and the Experimental Setup

4.4 Trapping of ^{85}Rb

Figure 14 depicts the trapping of ^{87}Rb atoms. As decided in 4.1, the experiment

is conducted using ^{85}Rb atoms. However, since the lab is most familiar with ^{87}Rb, ^{87}Rb atoms are used first to create a dipole trap to test the apparatus. Then, ^{85}Rb atoms are trapped.

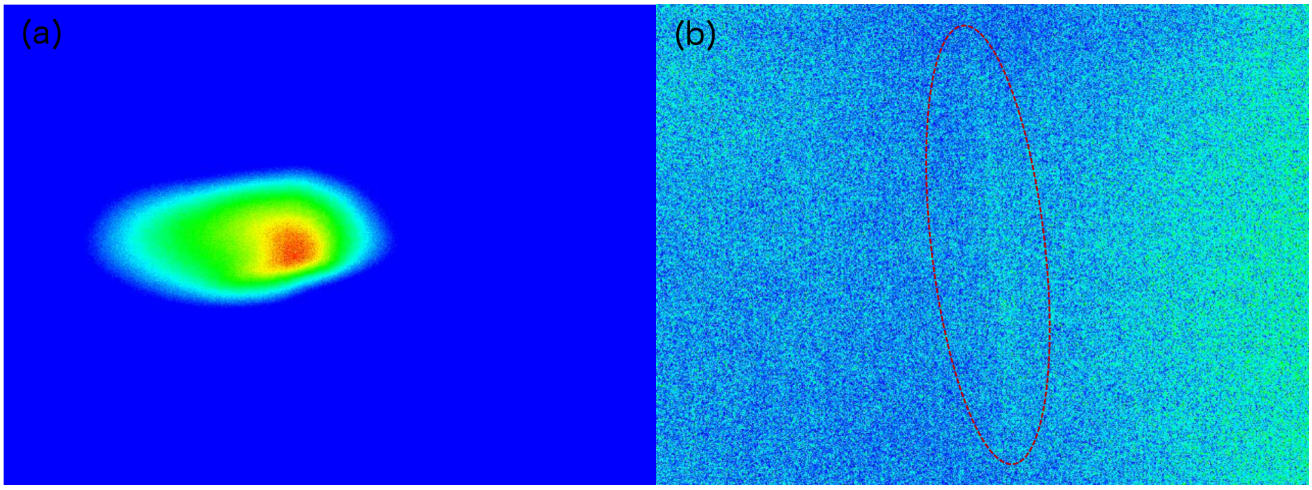

Figure 15: (a) ^{85}Rb MOT, (b) ^{85}Rb Dipole Trap. The red ellipse indicates the location of the very faint dipole trap.

First, the MOT of ^{85}Rb is constructed as shown in Figure 15 (a). Then, using lasers, the dipole trap is created with ^{85}Rb as shown in Figure 15 (b). However, this original dipole trap is not dense enough to observe Feshbach resonances. Thus, the density of the dipole trap is increased using various methods, as shown in Figure 16.

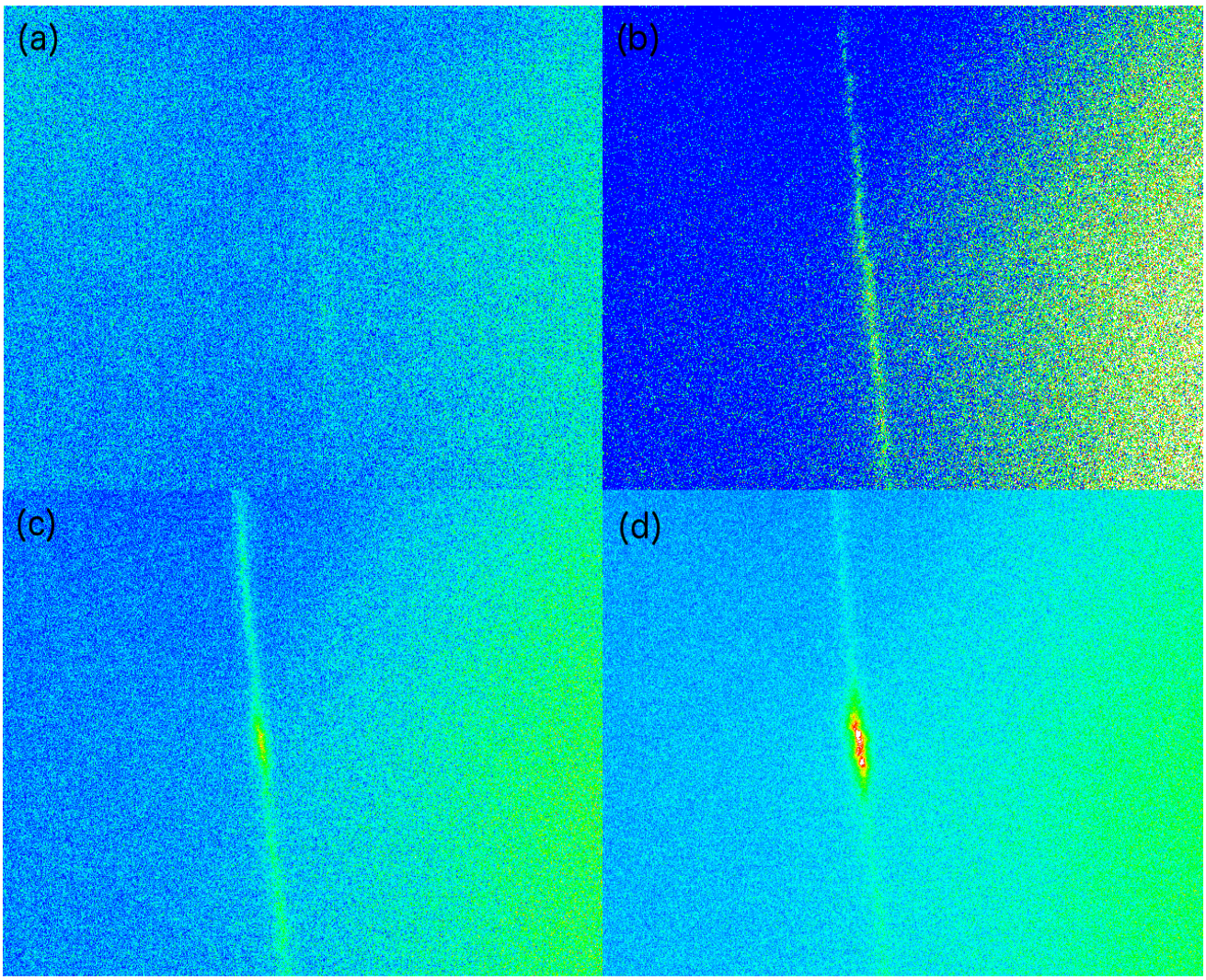

Figure 16: Evolution of the ^{85}Rb Dipole Trap. (a) the original dipole trap. (b) dipole trap with compressed MOT and better alignment. (c) retro-reflected cross dipole trap. (d) retro-reflected cross dipole trap with better alignment.

First, the MOT is compressed by increasing the applied magnetic field, and the laser is aligned better. The resulting is shown in Figure 16 (b). Then, the laser is retro-reflected to create a cross dipole trap. The experimental setup is shown in Figure 18 (b). The result is shown in Figure 16 (c). In this figure, the dipole trap became more compressed at the center. Then, the laser is better aligned so that the retro-reflected beam had maximal impact on the cross dipole trap. The

result is shown in Figure 16 (d). Moreover, the temperature measurement of the dipole trap is taken by measuring the width of the thermal cloud. The temperature measurement yields that the dipole trap is at around $T = 8\,\mu K$.

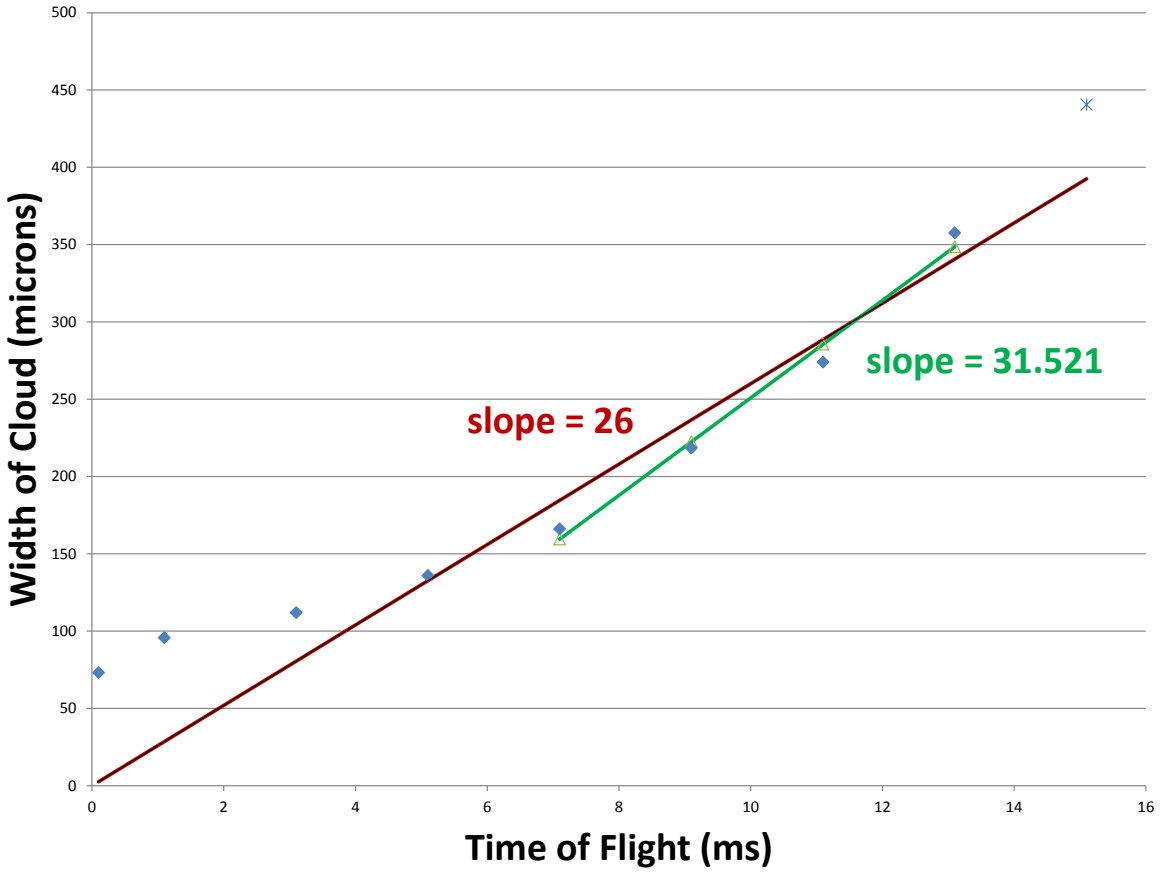

Figure 17: Temperature Measurement of the Dipole Trap in Figure 16 (d). The slope of the green fit yields the average velocity of the atoms in the thermal cloud. Then, this average velocity is used to calculate temperature, since $1/2mv^2 = 1/2kT$. The slope of the fitting function in green gives the average velocity of expansion, $v = 31.5\,\mu m/ms$. The red fit is used to calculate the error bar. The calculated error is 8.76 %.

Through these processes, we were able to create a dense dipole trap, but the observation of Feshbach resonances would require all of the atoms to participate. At this stage, only 20 percent of the atoms would contribute. In order to make all atoms contribute, the atoms all have to be in the same desired state. The ideal atomic state for ^{85}Rb atoms for Feshbach resonance observation is $F = 2$ and $m_F = -2$. In

order to obtain the atoms in a single quantum state, optical pumping is required. Furthermore, the platform for a second dipole trap laser is built and shown in Figure 18 (b).

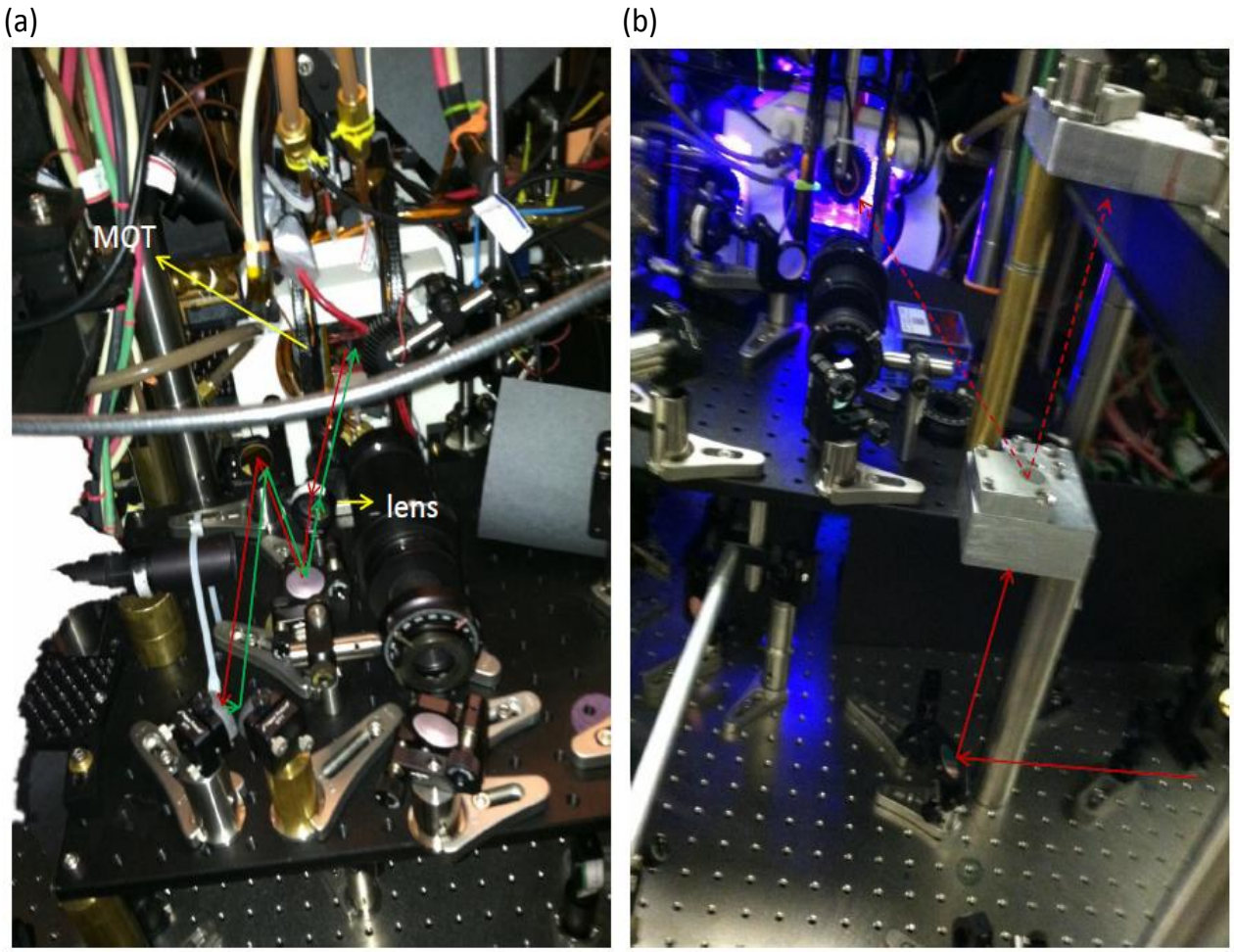

Figure 18: Experimental trapping laser setup. (a) Retro-reflected dipole trap scheme. (b) Planned path of the 2nd dipole trap laser for further compression of atoms. The aluminum platform features a hole for easy passage of the dipole trap laser beam

5. Conclusion

The objective of this project is to study and observe Feshbach resonances. There are two theoretical cornerstones of Feshbach resonances: the scattering of cold atoms

and the bound states. Thus, in order to develop a theoretical understanding of Feshbach resonances, scattering theory and bound states are studied. The phase shifts of a spherical well is both numerically and analytically modelled. The bound states of the well potential are studied. On the experimental side, atom pairs with favorable resonance widths and Feshbach magnetic field values were identified. The MOT and the dipole trap using ^{85}Rb and ^{87}Rb are constructed.

This study will facilitate the future observation of Feshbach resonance. Once the Feshbach resonances are observed, the association of atoms into molecular states can be investigated. On the theory side, the theory of Feshbach molecules may be investigated. The control of the resonance width in Feshbach resonances can also be a theoretical endeavour.

6. References

[1] Quemener, Goulven, and Paul S. Julienne. "Ultracold Molecules under Control!." Chemical Reviews 112.9 (2012): 4949-5011.

[2] Carr, Lincoln D., et al. "Cold and ultracold molecules: science, technology and applications." New Journal of Physics 11.5 (2009): 055049.

[3] C. Chin, R. Grimm, P. Julienne, E. Tiesinga, Feshbach resonances in ultracold gases. Rev. Mod. Phys. 82, 1225 (2010).

[4] Roberts, J. L., N. R. Claussen, S. L. Cornish, and C. E. Wie- man, 2000, Magnetic field dependence of ultracold inelas- tic collisions near a Feshbach resonance, Phys. Rev. Lett. 85, 728731.

[5] Simoni, A., M. Zaccanti, C. DErrico, M. Fattori, G. Roati, M. Inguscio, and G. Modugno, 2008, Near-threshold model for ultracold KRb dimers from interisotope Feshbach spectroscopy, Phys. Rev. A 77, 052705.

[6] Simoni, A., F. Ferlaino, G. Roati, G. Modugno, and M. Ingus- cio, 2003, Magnetic control of the interaction in ultracold K-Rb mixtures, Phys. Rev. Lett. 90, 163202.

[7] Ferlaino, F., C. DErrico, G. Roati, M. Zaccanti, M. Inguscio, G. Modugno, and A. Simoni, 2006, Feshbach spectroscopy of a K-Rb atomic mixture, Phys. Rev. A 73, 040702(R) , ibid 74, 039903(E).

[8] Mueller, Erich. "Scattering Tutorial." Mueller Research Group. Erich Mueller, 12 Aug. 2002. Web. 10 Apr. 2013.

A. Appendix- Source Codes

7.1 Matlab Codes for 1-D Attractive Well

```
function [E,rtx,rty,y1,y2,k] = attr_well(V_0)
%from the boundary condition, this function solves for energies, and
%intersections at varying well depths

m=1;%mass=1
a=2;%radius of well=2
start=0;
finish=10*pi/a;
step=.001;
k=start:step:finish;
%momentum scanned
k_0=sqrt(2*m*V_0);
%hbar set to 1

A=abs(cos(k.*a./2));
B=abs(sin(k.*a./2));
C=sign(tan(k.*a./2));

y1=A.*((1+C)./2)+B.*((1-C)./2);
%boundary condition

y2=k/k_0;
%another boundary condition

[rtx,rty]=rootfinder(k,y1,y2,step);
%y1 and y2 intersections, or where the boundary conditions are satisfied


%scan V_0 from 0 to 200
E=solve_for_E(m,k_0,rtx);
E=rid_the_doubles(E);

end
```

```
function [rootx, rooty] = rootfinder(k,f1,f2,step)
%make sure f1, f2, indept_var all have the same size!!!
%this function finds "roots," or more accurately, intersections of two given
%functions

[t,s]=size(f1);
if s<t
    s=t;
end
%so it doesnt matter if i pass an array or a vector

rootx=zeros(1,20);
rooty=zeros(1,20);
index=1;

for i=1:s
    if abs(f1(i)-f2(i))<(step)
        rootx(index)=k(i);
        rooty(index)=f2(i);
        index=index+1;
    end
end

    rootx=rootx(1:index-1);
    rooty=rooty(1:index-1);

end
```

```
function [E] = solve_for_E(m,k_0,rtx)
% this function solves the resulting momentum intersections to energies.
[s,t]=size(rtx);
if t<s
    t=s;
end
%so it doesnt matter if i pass an array or a vector

E=zeros(1,t);

for i=1:t
    E(i)=-((rtx(i))^2-(k_0)^2)/2*m;
end

end
```

```
function [E] = rid_the_doubles(E)
% this function gets rid of double counted intersections.
%if the spacing between two intersections is too small,
% then it only counts one intersection.

[x,y]=size(E);
if y<x
    y=x;
end
%so it doesnt matter if i pass an array or a vector

for i=1:(y-1)
   if abs(E(i)-E(i+1))<.6
       E(i+1)=E(i);
   end
end

E=unique(E);

end
```

The function below generates the Figure 4.

```
function [] = test_attr_well()
%this function plots the boundary conditions and intersections
%at different values of V_0

[E,rtx,rty,y1,y2,k]=attr_well(2);
plot_intersections(k,y1,y2,rtx,rty,1)
disp('(on figure 1) E when V_0=2 is: ')
disp(E)

[E,rtx,rty,y1,y2,k]=attr_well(20);
plot_intersections(k,y1,y2,rtx,rty,2)
disp('(on figure 2) E when V_0=20 is: ')
disp(E)

[E,rtx,rty,y1,y2,k]=attr_well(100);
plot_intersections(k,y1,y2,rtx,rty,3)
disp('(on figure 3) E when V_0=100 is: ')
disp(E)

[E,rtx,rty,y1,y2,k]=attr_well(200);
plot_intersections(k,y1,y2,rtx,rty,4)
disp('(on figure 4) E when V_0=200 is: ')
disp(E)

[E,rtx,rty,y1,y2,k]=attr_well(300);
plot_intersections(k,y1,y2,rtx,rty,5)
disp('(on figure 5) E when V_0=300 is: ')
disp(E)

end
```

```
function [] = plot_intersections(k,y1,y2,rtx,rty,number)
%this function plots two bdy conditions, limit, roots.

figure(number)
plot(k,y1)
hold on
    plot(k,y2,'g')
hold off
hold on
    plot(k,1,'r')
hold off
hold on
    scatter(rtx,rty,'o','m')
hold off

end
```

The function below generates the Figures 5 and 6.

```
function [] = E_vs_V(number)
%this function plots the bound state energies vs the well depth, V_0.
step=.01;
V_0=2:step:70;
[~,t]=size(V_0);
V=zeros(1,10*t); %scans V_0
E=zeros(1,10*t);
%as we solve for the energy levels, we will be filling this vector.
n=1;
m=1;

for i=1:t
    [E_0,~,~,~,~,~]=attr_well(V_0(i));
    [~,y]= size(E_0);
    a=1;

    for l=m:(m+y)
        V(l)=V_0(i);
    end
        m=m+y;
    for j=n:(n+y)
        if a<=y
            E(j)=E_0(a);
            a=a+1;
        end
    end
        n=n+y;
end

[~,d]=size(E);
V=V(1:d);

figure(number)
scatter(V,E,5,'.')
hold on
    E1=0;
    plot(V,E1)
hold off

end
```

7.2 Matlab Codes for 3-D Attractive Well Potential

```
function [E,rtx,rty,y1,y2,k] = attr_well(V_0)
%this function solves for intersections, or at what
%values of momentum the boundary conditions are satisfied.
m=1;
%mass=1
a=2;
%radius of well=1
start=0;
finish=10*pi/a;
step=.001;
k=start:step:finish;
k_p_squared=V_0-k.^2;
k_p=sqrt(k_p_squared);
k_p=real(k_p);

%the boundary conditions, y1 and y2
y1=cot(k_p.*a);
y2=-k./k_p;

%intersections
[rtx,rty]=rootfinder(k,y1,y2,step*30);

%scan V_0 from 0 to 200
E=solve_for_E(rtx);
E=rid_the_doubles(E);

end
```

This function uses the same functions solve_for_E, rid_the_doubles, and rootfinder from Appendix A.1. Using the same function test_attr_well generates Figure 7.

The function below plots Figures 8 and 9.

```
function [] = E_vs_V(number)
%this function plots the bound state energies at different values of V_0.
step=.01;
V_0=0.6:step:60;
%scans V_0
[~,t]=size(V_0);
V=zeros(1,10*t);
E=zeros(1,10*t);
n=1;
m=1;

for i=1:t
    [E_0,~,~,~,~,~]=attr_well(V_0(i));
    [~,y]= size(E_0);
    a=1;

    for l=m:(m+y)
        V(l)=V_0(i);
    end
        m=m+y;
    for j=n:(n+y)
        if a<=y
            E(j)=E_0(a);
            a=a+1;
        end
    end
        n=n+y;
end

[~,d]=size(E);
V=V(1:d);

V1=0:step:60;

figure(number)
scatter(V,E,5,'.')
hold on
    E1=0;
    plot(V1,E1)
hold off
axis([0 60 -1 30])
```

```
figure(number+1)
scatter(V,E,5,'.')
axis([0 5 -1 2])

hold on
    E1=0;
    plot(V1,E1)
hold off

end
```

7.3 Matlab Codes for Phase Plot

The Matlab function "phase" generates Figure 10.

```
function [] = phase()
%This function plots the phases vs momentum at varying well depths.

m=1;%mass set to 1
a=1;%radius of the well set to 1

start=0;
finish=5*pi/a;
step=.001;
k=start:step:finish;

q=0:0.1*pi:5*pi;

n=(q-rem(q,pi))./pi;

[~,c]=size(n);

l=round(q./pi);

figure;

for i=1:c
    done=0;
    V_0=(q(i).^2)./(2*m);

    [delta]=sph_attr_well2(V_0);
    while done==0
        [delta,done]=scale(delta,1);
    end

    if i>1
        if l(i)-l(i-1)==1
            delta=delta+(2*l(i)-1)*pi/2;
        else
            delta=delta+l(i)*pi;
        end
    end


    hold on
    plot(k,delta)
```

```
    hold off

end


end
```

```
function [y3] = sph_attr_well2(V_0)
%this function determines the boundary condition using phase shifts.
a=1;%radius=1
start=0;
finish=5*pi/a;
step=.001;

k=start:step:finish;

k_p=sqrt(k.^2+2*V_0);

S_p=sin(k_p.*a);
C=cos(k.*a);
S=sin(k.*a);
C_p=cos(k_p.*a);

A=k.*S_p.*C;
B=k_p.*S.*C_p;
D=k_p.*C_p.*C;
E=k.*S.*S_p;
%boundary conditions
y1=(A-B)./(D+E);

y3=atan(y1);

end
```

```
function [A,done] = scale(A,step)
%this function scales the phase by getting rid of discontinuities
%that arise from taking arctangent
[~,b]=size(A);
done=0;
c=0;


for i=1:b

    if (i+1)>b
       done=1;
       c=-1;
       return;
    end
    if abs(A(i)-A(i+1))>step
       change=abs(A(i)-A(i+1));
       c=i;
       break;
   end
end

if (c>0)&&(c+1<b)
for i=c+1:b
    A(i)=A(i)-change;
end
end

end
```

7.4 Matlab Codes for Scattering Length Plot

```
function [V,A] = iterate_pi_slength(number,n)
%this function solves for the scattering length from phase
a=1;%radius=1
m=1;%mass=1


start=0;
finish=5*pi/a;
step=.001;
k=start:step:finish;%momentum scanned

start=number*pi-2;
finish=number*pi+2;
step=.0003*pi/a;
q=start:step:finish;%q is used to scan V_0

[~,c]=size(q);

V=zeros(1,c);
A=zeros(1,c);
j=1;

for i=1:c
    done=0;
    V_0=(q(i).^2)./(2*m);

    [delta]=sph_attr_well2(V_0);
    delta=delta+number*pi;

    y=tan(delta)./k;


    V(j)=V_0;
    A(j)=y(n);
    j=j+1;


end
end
```

```
function [j,x] = diverge_at(V,A)
%this function figures out where the input function diverges.
[~,b]=size(A);
%j=index
j=0;
for i=1:b
   if (sign(A(i)) ~= sign(A(i+1)))&&(abs(A(i)-A(i+1))>100)
       j=i;
       break;
   end
end

x=(V(j)+V(j+1))/2;

end
```

The function below generates the Figures 11 and 13.

```
function [] = A_vs_V()

[V,A]=iterate_pi_slength(1,2);
figure;
scatter(V,A,'.','b');
[~,x_0]=diverge_at(V,A);
hold on
x=0:.001:200;
plot(x, -1./(x-x_0),'b')
x_0
hold off

[V,A]=iterate_pi_slength(2,2);
figure;
scatter(V,A,'.','b');
[~,x_0]=diverge_at(V,A);
hold on
x=0:.001:200;
plot(x, -1./(x-x_0),'b')
x_0
hold off

[V,A]=iterate_pi_slength(3,2);
figure;
scatter(V,A,'.','b');
[~,x_0]=diverge_at(V,A);
hold on
x=0:.001:200;
plot(x, -1./(x-x_0),'b')
x_0
hold off

[V,A]=iterate_pi_slength(4,2);
figure;
scatter(V,A,'.','b');
[~,x_0]=diverge_at(V,A);
hold on
x=0:.001:200;
plot(x, -1./(x-x_0),'b')
x_0
hold off
```

```
[V,A]=iterate_pi_slength(5,2);
figure;
scatter(V,A,'.','b');
[~,x_0]=diverge_at(V,A);
hold on
x=0:.001:200;
plot(x, -1./(x-x_0),'b')
x_0
hold off



end
```